IEEE Access
Multidisciplinary ⋮ Rapid Review ⋮ Open Access Journal

Received November 18, 2020, accepted December 8, 2020, date of publication December 18, 2020,
date of current version December 31, 2020.

Digital Object Identifier 10.1109/ACCESS.2020.3045789

A Novel Practical Robust Control Inheriting PID for SCARA Robot

SHENGCHAO ZHEN[1,2], (Member, IEEE), ZIYI ZHAO[1,2], XIAOLI LIU[1,2], (Student Member, IEEE), FENG CHEN[3], HAN ZHAO[1,2], AND YE-HWA CHEN[4,5], (Member, IEEE)

[1]School of Mechanical Engineering, Hefei University of Technology, Hefei 230009, China
[2]Anhui Key Laboratory of Digital Design and Manufacturing, Hefei University of Technology, Hefei 230009, China
[3]Institute of Advanced Manufacturing Engineering, Hefei University, Anhui 230022, China
[4]George W. Woodruff School of Mechanical Engineering, Georgia Institute of Technology, Atlanta, GA 30332, USA
[5]Key Laboratory of Road Construction Technology and Equipment of MOE, Chang'an University, Xi'an 710064, China

Corresponding author: Xiaoli Liu (xiaolihfut@qq.com)

This work was supported in part by the University Synergy Innovation Program of Anhui Province under Grant GXXT-2019-031, in part by the Natural Science Fund of Education Department of Anhui Province under Grant KJ2016A590, in part by the Fundamental Research Funds for the Central Universities of China under Grant PA2020GDSK0091, and in part by the Fundamental Research Funds for the Central Universities under Program 300102258305.

ABSTRACT In this paper, we propose a novel practical robust control algorithm for the Selective Compliance Articulated Robot Arm (SCARA) robot and verify the effectiveness through experiments. The dynamic model of the SCARA robot is established considering uncertainties, which include the nonlinear friction, parameter uncertainty, and external disturbance. To restrain the reversal chattering, we apply a modified Stribeck friction model with Gaussian compensation term as the friction description. The algorithm is composed of a proportional-derivative (PD) feedback term based on the model and a robust term. The formation of the robust part comprises the upper bound of the uncertainty. The Lyapunov minimax method is adopted to prove that the system is uniformly bounded and uniformly ultimately bounded, thus guaranteeing the practical stability of the system. Moreover, rapid controller prototyping cSPACE, as the experimental platform, can eliminate the tedious programming work and provide a great convenience for the experiments. The experimental results indicate that the robust control algorithm has good performance, which provides accurate trajectory tracking under the influence of uncertainties.

INDEX TERMS SCARA robot, robust control, uncertainty, nonlinear friction.

I. INTRODUCTION

In recent years, the trend of replacing humans with robots is on the rise with the rapid development of the Computer, Communication, and Consumer Electronic (3C) industry. Selective Compliance Articulated Robot Arm (SCARA) robot plays an increasingly important role in 3C assembly, welding, and handling with its high speed, short cycle, accurate path control, and reliable flexible operation [1], [2]. Due to the characteristics of fast action beat in the 3C industry, we need dynamic control of the SCARA robot to ensure its accuracy. Nevertheless, SCARA robot is difficult to control with its time-varying, strong coupling, and other dynamic characteristics. Therefore, using the traditional control algorithms to deal with the uncertainties of the complex system cannot get satisfactory results.

The associate editor coordinating the review of this manuscript and approving it for publication was Hai Wang.

During the past decades, there have been many typical algorithms to build up the accurate tracking performance of robot system, such as proportional-integral-derivative (PID) control [3]–[5], robust control [6], [7], sliding mode control [8], [9], adaptive control [10]–[12], fuzzy control [13], [14], genetic algorithm and particle swarm optimization [15], [16] and so on. Each algorithm has its advantage and limitation. PID control is widely used due to its low dependence on the dynamic model, whereas it is not satisfactory in the case of nonlinear friction and external interference. Based on PID control, a dual-loop control with active disturbance rejection control (ADRC) was proposed in [17] to achieve stable control of the robot. Sliding mode control is prone to chattering, which affects the tracking accuracy. [18] proposed a robust recursive sliding mode controller combined with an adaptive disturbance observer, which eliminates the system chattering in the reaching control input. Adaptive control is considered to be more suitable for the uncertainty

of the system but requires high real-time performance. Fuzzy control and neural network control, which are based on the data model rather than the mathematical model, make their precision difficult to meet the high accuracy requirements of 3C industry. Moreover, [19] proposed a tracking control scheme with radial basis function (RBF) neural network, which combines the incremental PID control and sliding mode control. [20] used an adaptive inertia weight particle swarm optimization. [21] proposed a hybrid coordinated control based on port-controlled Hamiltonian and backstepping. In engineering, working environment of the robot is complex, where uncertainties are increasing and hard to predict. In order to solve engineering problems better, a practical and effective control scheme needs to be proposed.

Robust control is widely used for its strong robustness to system uncertainties and simple implementation. [22] proposed an adaptive recursive terminal sliding-mode controller to make the tracking error converge to zero in a finite time. [23] proposed a hierarchical sliding mode control with perturbation estimation technique on a two-wheeled self-balancing vehicle, which achieved good balancing and velocity tracking performance even under external disturbances. It is important to explore a practical and effective robust control algorithm for the SCARA robot in engineering applications. Since robust control has characteristic advantages in dealing with model uncertainties and external disturbance, we aim to come up with a novel practical robust control scheme in this paper via a creative description of uncertainties. An adaptive model-free control (AMC) in [24] can make the tracking error converge to a region in finite time. AMC scheme is more complicated in practical applications, because of the need to design and adjust the adaptive law. Relatively speaking, the advantages of the proposed algorithm are simple structure, few tuning parameters, and simple tuning process. The system is divided into a nominal part and an uncertain part. The uncertainties of SCARA robot system are nonlinear time-varying but bounded. The proposed algorithm is composed of a PD feedback term based on the model and a robust term. The formation of the robust term comprises the upper bound of the uncertainties. The Lyapunov minimax method is employed to prove that the controller is uniformly bounded and uniformly ultimately bounded, thus ensuring the practical stability of the system.

In this paper, the main contributions are three parts. First, we propose a specific robust controller and apply the modified Stribeck friction model with Gaussian compensation term as the friction description to reduce the reversal chattering caused by nonlinear friction in motion. Second, the Lyapunov minimax method is adopted to prove the actual stability of the system. Finally, the numerical simulation and experimental verification, comparing with other algorithms, are carried out based on the SCARA robot. The results indicate that the proposed algorithm has good performance, which provides accurate trajectory tracking under the influence of uncertainties.

II. THE ESTABLISHMENT OF DYNAMIC MODEL OF SCARA ROBOT

We choose a kind of 4-DOF SCARA robot as the research object. The four degrees of freedom are lifting motion, joint 1 rotation, joint 2 rotation, and terminal rotation. Since there is no coupling between the lifting motion and other motions, it can be considered separately. Meanwhile, the robot is mainly focused on end-position control, so the terminal rotational motion has little influence on the research results and can be ignored. The two degrees of freedom of the joint 1 and 2 on the plane are coupled to each other, and the positioning of the robot is mainly guaranteed by the two rotating joints. Therefore, the robot is simplified to a planar two-degree-of-freedom manipulator.

The schematic representation of the simplified SCARA robot model is shown in Fig.1, where m_1 and m_2 are masses of link 1 and link 2, m_3 is the mass of the motor of joint 2, m_4 is the mass of the end components (including the end motor), l_1 is the length of the link 1, l_2 is the length of the link 2, c_1 is the distance from the center of mass of the link 1 to point O, c_2 is the distance from the center of mass of the link 2 to point A, l_3 is the distance from the motor of the joint 2 to point O.

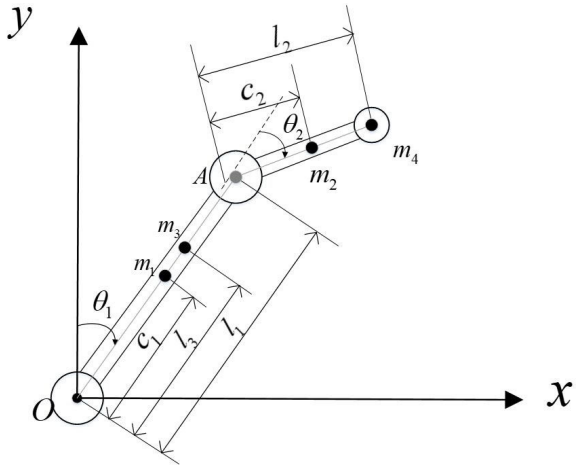

FIGURE 1. The schematic representation of the simplified SCARA robot model.

Newton-Euler method and Lagrangian method are the representative methods in the dynamic modeling of robots. When solving the dynamics problem, the Lagrangian method only needs to find out the kinetic energy and potential energy of the whole system, which is simple and easy to be expressed. Therefore, we choose the Lagrangian method to establish the dynamical model. $[\theta_1, \theta_2]^T$ are two coordinates that are independent of each other to describe the rotation angles of joint 1 and joint 2. The total energy includes kinetic energy and potential energy of all independent parts of the system. The Lagrange equation of the system is

$$\frac{d}{dt}\left(\frac{\partial L}{\partial \dot{q}}\right) - \frac{\partial L}{\partial \dot{q}} = \tau - \tau_f, \tag{1}$$

where the Lagrangian $L = T - V$, T is the kinetic energy and V is the potential energy, q, $\dot{q}$ are generalized coordinates

and generalized velocities respectively, τ is the control output, and τ_f is the friction and external disturbances torque. We have

$$\begin{aligned} T = &\frac{1}{2}J_1\dot{\theta}_1^2 + \frac{1}{2}m_2[\dot{\theta}_1^2 l_1^2 + c_2^2(\dot{\theta}_1+\dot{\theta}_2)^2 \\ &+ 2\dot{\theta}_1 l_1 c_2 cos\theta_2(\dot{\theta}_1+\dot{\theta}_2)] + \frac{1}{2}J_2(\dot{\theta}_1+\dot{\theta}_2)^2 \\ &+ \frac{1}{2}m_3(\dot{\theta}_1 l_3)^2 + \frac{1}{2}m_4[\dot{\theta_1}^2 l_1^2 + l_2^2(\dot{\theta}_1 \\ &+ \dot{\theta}_2 cos\theta_2)]. \end{aligned} \tag{2}$$

Because the SCARA robot is simplified to a planar robot, the potential energy $V = 0$. Substituting the kinetic energy into the Lagrange equation, we have the dynamic equation of SCARA robot system

$$M(q)\ddot{q} + C(q,\dot{q})\dot{q} + G(q) + F(q,\dot{q}) = \tau, \tag{3}$$

where $M(q)$ is the inertia matrix, $C(q,\dot{q})$ is the Coriolis/centrifugal force matrix, $G(q)$ is the Gravity vector, $F(q,\dot{q})$ is the friction force and external disturbances.

$$q = \begin{bmatrix}\theta_1\\ \theta_2\end{bmatrix}, \quad \dot{q} = \begin{bmatrix}\dot{\theta}_1\\ \dot{\theta}_2\end{bmatrix}, \ddot{q} = \begin{bmatrix}\ddot{\theta}_1\\ \ddot{\theta}_2\end{bmatrix}, \tau = \begin{bmatrix}\tau_1\\ \tau_2\end{bmatrix} \tag{4}$$

$$M(q) = \begin{bmatrix}M_{11} & M_{12}\\ M_{21} & M_{22}\end{bmatrix} \tag{5}$$

$$\begin{aligned} M_{11} &= I_1 + I_2 + (m_2+m_4)l_2^2 + m_3 l_3^2 + m_2 c_2^2 \\ &\quad + m_4 l_2^2 + 2(m_2 l_1 c_2 + m_4 l_1 l_2)cos\theta_2 \end{aligned} \tag{6}$$

$$\begin{aligned} M_{12} &= M_{21} \\ &= I_2 + m_2 c_2^2 + m_4 l_2^2 \\ &\quad + (m_2 l_1 c_2 + m_4 l_1 l_2)cos\theta_2 \end{aligned} \tag{7}$$

$$M_{22} = I_2 + m_2 c_2^2 + m_4 l_2^2 \tag{8}$$

$$C(q,\dot{q}) = \begin{bmatrix}C_{11} & C_{12}\\ C_{21} & C_{22}\end{bmatrix} \tag{9}$$

$$C_{11} = -2(m_2 l_1 c_2 + m_4 l_1 l_2)sin\theta_2\ddot{\theta}_2 \tag{10}$$

$$C_{12} = -(m_2 l_1 c_2 + m_4 l_1 l_2)sin\theta_2\ddot{\theta}_2 \tag{11}$$

$$C_{21} = (m_2 l_1 c_2 + m_4 l_1 l_2)sin\theta_2\ddot{\theta}_1 \tag{12}$$

$$C_{22} = 0. \tag{13}$$

Since the two axes of the SCARA robot move in the horizontal plane, the gravity does not influence the system. We have $G(q) = [0,0]^T$. For F, we have $F = F_{fric} + F_d$, where the F_{fric} denotes the nonlinear friction force and the F_d denotes the external disturbances.

Assumption 1: The inertia matrix $M(\cdot)$ in the SCARA robot system is uniform positive definite for all θ, which means that there are scalar constants $\underline{\gamma}, \bar{\gamma} > 0$ such that

$$0 < \underline{\gamma} I \le M(\cdot) \le \bar{\gamma} I, \tag{14}$$

Theorem 1: The matrix $\dot{M}(\cdot) - 2C(\cdot)$ is skew symmetric for all $\theta, \dot{\theta}$ [25]. That is, for any vector ξ, there is

$$\xi^T \left\{\dot{M}(\cdot) - 2C(\cdot)\right\}\xi = 0. \tag{15}$$

In the process of robot movement, due to unreasonable structure design, insufficient lubrication, or too tight assembly, the nonlinear friction of joints has a particularly great impact on the movement of the robot. It affects both the dynamic and static performance of the system, causing problems such as system creep and limit cycle oscillation, especially when the system is moving at a low speed. Therefore, the establishment of a correct and effective friction model can greatly improve joint control performance. In many pieces of research, the friction model is directly treated as Coulomb-Viscous friction model or Stribeck friction model. These models are simple and effective, and the parameters are easy to identify, but they can only describe the static characteristics of friction at a constant speed and cannot deal with the friction when reversing. In this case, we use a modified Stribeck friction model with Gaussian compensation term in commutation [26]. The friction can be described as

$$\begin{aligned} F_{fric}(\dot{q}_i(t)) = &[f_{ci} + (f_{si} - f_{ci})e^{-(\dot{\theta}_i/\omega_s)^2}]sgn(\dot{\theta}_i) \\ &+ f_{vi}\dot{\theta}_i - f_{gi}, \quad i = 1,2, \end{aligned} \tag{16}$$

where f_{ci} is the Coulomb Friction coefficient, f_{si} is the Static Friction coefficient, f_{vi} is viscous friction coefficient, ω_s is Stribeck velocity and f_{gi} is the Gaussian function. For f_{gi}, we have

$$\begin{cases} f_{gi} = s_i e^{-(\dot{\theta}_i/v_i)^2} \\ s_i = sgn(\dfrac{\dot{\theta}_i}{a_i})f_{si} + f_{ci}l \\ v_i = a_i\omega_s[d\cdot sgn(a) + c\cdot sgn(\dot{\theta}_i)], \quad i = 1,2 \end{cases} \tag{17}$$

where a_i is the acceleration at the output of the corresponding motor and l, d, c are all parameters that need to be identified.

Considering the manufacturing assembly, external disturbance, and other factors, there are uncertainties in the system. The dynamic model of the system can be described as

$$M(\theta,\sigma,t)\ddot{\theta}(t) + C(\theta,\dot{\theta},\sigma,t)\dot{\theta}(t) + F(\dot{\theta},\sigma,t) = \tau(t) \tag{18}$$

where $\sigma \in \sum \subset R^n$ is the uncertain parameter, the set $\sum \subset R^n$, which means the bound of σ, is assumed to be known and compact. We assume the uncertainties are time-varying but bounded.

III. CONTROLLER DESIGN AND STABILITY ANALYSIS

A. CONTROLLER DESIGN

Robot dynamic control should make each joint of the robot have good performance in tracking a given trajectory. The robust controller for the SCARA robot is designed to suppress the influence of various uncertainties and make the tracking error converge to zero gradually.

For the SCARA robot, $\theta^d(t)$, $t \in [t_0, t_1]$ is the given trajectory, with the desired velocity and acceleration $\dot{\theta}^d(t)$, $\ddot{\theta}^d(t)$. Assume $\theta^d : [t_0,\infty) \to R^n$, is of class C^2 and they are uniformly bounded. We define the tracking error as:

$$e(t) = \theta(t) - \theta^d(t), \tag{19}$$

then we can get

$$\dot{e}(t) = \dot{\theta}(t) - \dot{\theta}^d(t), \ddot{e}(t) = \ddot{\theta}(t) - \ddot{\theta}^d(t). \tag{20}$$

The tracking error vector can be writen as

$$\hat{e}(t) = [e(t), \dot{e}(t)]^T. \tag{21}$$

Therefore, we are supposed to propose a controller to make the tracking error vector $\hat{e}$ of the SCARA robot system uniformly bounded and uniformly ultimately bounded.

Moreover, the equation (18) can be rewritten as

$$M(\theta, \sigma, t)(\ddot{\theta}^d(t) + \ddot{e}(t)) + C(\theta, \dot{\theta}, \sigma, t)(\dot{\theta}^d(t) + \dot{e}(t)) + F(\dot{\theta}, \sigma, t) = \tau(t). \tag{22}$$

The functions $M(\cdot)$, $C(\cdot)$ and $F(\cdot)$ consist of two parts

$$M(\theta, \sigma, t) = \bar{M}(\theta, t) + \Delta M(\theta, \sigma, t), \tag{23}$$
$$C(\theta, \dot{\theta}, \sigma, t) = \bar{C}(\theta, \dot{\theta}, t) + \Delta C(\theta, \dot{\theta}, \sigma, t), \tag{24}$$
$$F(\dot{\theta}, \sigma, t) = \bar{F}(\dot{\theta}, t) + \Delta F(\dot{\theta}, \sigma, t), \tag{25}$$

where $\bar{M}(\cdot)$, $\bar{C}(\cdot)$ and $\bar{F}(\cdot)$ are the nominal portions, whereas $\Delta M(\cdot)$, $\Delta C(\cdot)$ and $\Delta F(\cdot)$ are the uncertain portions which depend on σ. We now define a vector

$$\begin{aligned}\Phi(e, \dot{e}, \sigma, t) := &-\Delta M(\theta, \sigma, t)(\ddot{\theta}^d - S\dot{e}) \\ &- \Delta C(\theta, \dot{\theta}, \sigma, t)(\dot{\theta}^d - Se) \\ &- \Delta F(\dot{\theta}, \sigma, t),\end{aligned} \tag{26}$$

where $S = diag[s_1, s_2]$, $s_1, s_2 > 0$ are constants. Obviously $\Phi \equiv 0$ if all uncertainties disappear. Then, we choose a scalar ρ based on the assumed bound of model uncertainty and external disturbances, such that

$$\| \Phi(e, \dot{e}, \sigma, t) \| \leq \rho(e, \dot{e}, \sigma, t). \tag{27}$$

In the absence of special stated, $\| \cdot \|$ is always treated as the Euclidean norm.

The trajectory following problem of the SCARA robot to be solved is to design a controller $\tau(t)$. The proposed controller should ensure the $e(t)$ remains within the predetermined boundary. [27] proposed an approach of guaranteeing prescribed performance bounds. The deterministic robust control scheme can be expressed as

$$\tau(t) = \bar{M}(\ddot{\theta}^d - S\dot{e}) + \bar{C}(\dot{\theta}^d - Se) + \bar{F} - Pe - D\dot{e} - \frac{\beta}{\eta + \epsilon}, \tag{28}$$

where $P = \text{diag}\ [k_{pi}]_{2\times 2}$, $k_{pi} > 0$, $D = \text{diag}[k_{di}]_{2\times 2}$, $k_{di} > 0, i = 1, 2$ are proportional and differential parameters, which play a similar role to nominal PD control. ϵ is a positive design parameter, and

$$\beta = \gamma^2(\dot{e} + Se)\rho^4 \| \dot{e} + Se \|^2, \tag{29}$$
$$\eta = \gamma \| \dot{e} + Se \|^2 \rho^2, \tag{30}$$

where the scalars γ and ρ are positive design parameters. The values of ρ and γ depend on the practical engineering application. The controller (28) ensures $\hat{e}(t)$ of the system (22) to be uniformly bounded and uniformly ultimately bounded. Moreover, we can make the ultimate boundedness ball small enough by choosing the suitable design parameters.

B. PROOF OF STABILITY

The stability of the system can be proved by the Lyapunov minimax method. First, we choose a Lyapunov function candidate and prove the validity of it [28]. The Lyapunov function candidate is chosen as

$$V(\hat{e}) = \frac{1}{2}(\dot{e} + Se)^T M(\dot{e} + Se) + \frac{1}{2}e^T(P + SD)e. \tag{31}$$

Obviously $V(\hat{e})$ is legitimate if we can prove that $V(\hat{e})$ is (globally) positive definite and decrescent.

From Eq.(14), M is bounded, thus

$$\begin{aligned}V(\hat{e}) &\geq \frac{1}{2}\underline{\gamma} \| \dot{e} + Se \|^2 + \frac{1}{2}e^T(P + SD)e \\ &= \frac{1}{2}\underline{\gamma}\sum_{i=1}^{n}(\dot{e}_i^2 + 2s_i\dot{e}_i e_i + s_i^2 e_i^2) \\ &\quad + \frac{1}{2}\sum_{i=1}^{n}(k_{pi} + s_i k_{di})e_i^2 \\ &= \frac{1}{2}\sum_{i=1}^{n}[e_i \quad \dot{e}_i]\Psi_i \begin{bmatrix} e_i \\ \dot{e}_i \end{bmatrix},\end{aligned} \tag{32}$$

where

$$\Psi_i = \begin{bmatrix} \underline{\gamma}s_i^2 + k_{pi} + s_i k_{di} & \underline{\gamma}s_i \\ \underline{\gamma}s_i & \underline{\gamma} \end{bmatrix}. \tag{33}$$

It is easy to prove that $\Psi_i > 0, \forall i$. Thus V is positive definite.

$$V(\hat{e}) \geq \frac{1}{2}\sum_{i=1}^{n}\lambda_{min}(\Psi_i)(e_i^2 + \dot{e}_i^2) \geq \underline{\lambda}||\hat{e}||^2, \tag{34}$$

where $\underline{\lambda} = \min\left\{\frac{1}{2}\lambda_{min}(\Psi_1), \frac{1}{2}\lambda_{min}(\Psi_2)\right\}$, $\underline{\lambda} > 0$. By Assumption 1, there is

$$V(\hat{e}) \leq ||\dot{e} + Se||^2\bar{\gamma} + e^T(P + SD)e. \tag{35}$$

For the first term on the right-hand side,

$$\begin{aligned}\bar{\gamma}||\dot{e} + Se||^2 &= \bar{\gamma}(\dot{e} + Se)^T(\dot{e} + Se) \\ &= \bar{\gamma}[e \quad \dot{e}]\begin{bmatrix} S^2 & S \\ S & I \end{bmatrix}\begin{bmatrix} e \\ \dot{e} \end{bmatrix} \\ &\leq \bar{\gamma}\lambda_{max}\left(\begin{bmatrix} S^2 & S \\ S & I \end{bmatrix}\right)||\hat{e}||^2 \\ &=: \bar{\gamma}\bar{s}||\hat{e}||^2.\end{aligned} \tag{36}$$

For the second term, by Rayleigh's principle,

$$e^T(P + SD)e \leq \lambda_{max}(P + SD)||e||^2 \tag{37}$$

With Inequalities (35) and (36) into Inequality (34), we have

$$V(\hat{e}) \leq \bar{\gamma}\bar{s}||\hat{e}||^2 + \lambda_{max}(P + SD)||e||^2 =: \bar{\lambda}||\hat{e}||^2, \tag{38}$$

where $\bar{\lambda} = \bar{\gamma}\bar{s} + \lambda_{max}(P + SD)$. Note that $\bar{\lambda}$ in Inequality (38) is a strictly positive constant, which proves that $V(\hat{e})$ is decrescent. Therefore, it can be proved that $V(\hat{e})$ is a valid Lyapunov function candidate from (34) and (38).

Then, we prove the stability of the system. The time derivative of $V(\hat{e})$ is given by

$$\dot{V}(\hat{e}) = (\dot{e} + Se)^T M(\ddot{e} + S\dot{e}) + \frac{1}{2}(\dot{e} + Se)^T \dot{M}(\dot{e} + Se) + e^T(P + SD)\dot{e}, \quad (39)$$

for $\ddot{e} = \ddot{q} - \ddot{q}^d$ and Eq.(3), the first two terms become

$$\begin{aligned}
&(\dot{e} + Se)^T M(\ddot{e} + S\dot{e}) + \frac{1}{2}(\dot{e} + Se)^T \dot{M}(\dot{e} + Se) \\
&= (\dot{e} + Se)^T (M\ddot{q} - M\ddot{q}^d + MS\dot{e} + \frac{1}{2}\dot{M}(\dot{e} + Se)) \\
&= (\dot{e} + Se)^T (\tau - C(\dot{q}^d - Se) - G - F \\
&\quad - M\ddot{q}^d + MS\dot{e} - C(\dot{e} + Se) + \frac{1}{2}\dot{M}(\dot{e} + Se)) \\
&= (\dot{e} + Se)^T (\tau - C(\dot{q} - Se) - G - F - M\ddot{q}^d \\
&\quad + MS\dot{e}) + (\dot{e} + Se)^T (\frac{1}{2}\dot{M} - C)(\dot{e} + Se). \quad (40)
\end{aligned}$$

With Theorem 1, Eqs.(22) and (28), we can get

$$\begin{aligned}
&(\dot{e} + Se)^T M(\ddot{e} + S\dot{e}) + \frac{1}{2}(\dot{e} + Se)^T \dot{M}(\dot{e} + Se) \\
&= (\dot{e} + Se)^T (\tau - C(\dot{q} - Se) - G - T - M\ddot{q}^d + MS\dot{e}) \\
&\quad (\dot{e} + Se)^T (\bar{M}(\ddot{q}^d - S\dot{e}) - M(\ddot{q}^d - S\dot{e}) + \bar{C}(\dot{q}^d - Se) \\
&\quad - C(\dot{q}^d - Se) + \bar{G} - G + \bar{F} - F - \frac{\beta}{\eta + \epsilon} \\
&\quad - Pe - D\dot{e}) \\
&= (\dot{e} + Se)^T (-\Delta M(\ddot{q}^d - S\dot{e}) - \Delta C(\dot{q} - Se) \\
&\quad - \Delta G - \Delta F - \frac{\beta}{\eta + \epsilon} - Pe - D\dot{e}) \quad (41)
\end{aligned}$$

By Eqs.(26) and (27), we have

$$\begin{aligned}
&(\dot{e} + Se)^T M(\ddot{e} + S\dot{e}) + \frac{1}{2}(\dot{e} + Se)^T \dot{M}(\dot{e} + Se) \\
&= (\dot{e} + Se)^T [\Phi - \frac{\beta}{\eta + \epsilon} - Pe - D\dot{e}] \\
&\leq \| \dot{e} + Se \| \| \Phi \| - (\dot{e} + Se)^T (Pe + D\dot{e}) \\
&\quad - (\dot{e} + Se)^T \frac{\beta}{\eta + \epsilon}. \quad (42)
\end{aligned}$$

Since

$$\begin{aligned}
&-(\dot{e} + Se)^T \frac{\beta}{\eta + \epsilon} \\
&= -\frac{\| \dot{e} + Se \|^4 \gamma^2 \rho^4}{\eta + \epsilon} = -\frac{\eta^2}{\eta + \epsilon} \leq -\frac{\eta^2 - \epsilon^2}{\eta + \epsilon} \\
&= -\frac{(\eta + \epsilon)(\eta - \epsilon)}{\eta + \epsilon} = -\gamma \| \dot{e} + Se \|^2 \rho^2 + \epsilon, \quad (43)
\end{aligned}$$

and

$$-(\dot{e} + Se)^T (Pe + D\dot{e}) = -e^T PSe - \dot{e}^T D\dot{e} - e^T (P + SD)\dot{e}. \quad (44)$$

Substitute (43) and (44) into (42) and combine (39)

$$\begin{aligned}
\dot{V}(\hat{e}) &\leq \rho \| \dot{e} + Se \| - \gamma\rho^2 \| \dot{e} + Se \|^2 + \epsilon - e^T PSe \\
&\quad - \dot{e}^T D\dot{e} - e^T (P + SD)\dot{e} + e^T (P + SD)\dot{e} \\
&\leq \frac{1}{4\gamma} + \epsilon - e^T PSe - \dot{e}^T D\dot{e} \\
&\leq \frac{1}{4\gamma} - \lambda ||\hat{e}||^2 + \epsilon, \quad (45)
\end{aligned}$$

where $\lambda = \min\{\lambda_{min}(PS), \lambda_{min}(D)\}$. It shows that $\dot{V}$ is negative definite for all $||\hat{e}||$ such that

$$\frac{1}{4\gamma} - \lambda ||\hat{e}||^2 + \epsilon < 0. \quad (46)$$

Both $\gamma, \lambda, \epsilon$ are crisp. Thus, $\dot{V}(\hat{e})$ is negative for sufficiently large $||\hat{e}||$.

Thus, the controller (28) can ensure the uniform boundedness and uniform ultimate boundedness of the SCARA robot system (18). The uniform boundedness is guaranteed with the following performance. That is, for any $y > 0$ with $||\hat{e}(t_0)|| > 0$, we have

$$d(y) = \begin{cases} y\sqrt{\frac{\bar{\lambda}}{\underline{\lambda}}}, & y > Y, \\ Y\sqrt{\frac{\bar{\lambda}}{\underline{\lambda}}}, & y \leq Y, \end{cases} \quad (47)$$

$$Y = \sqrt{\frac{1}{4\gamma y}}, \quad (48)$$

such that $||\hat{e}(t)|| \leq d(y)$ for all $t \geq t_0$. Uniform ultimate boundedness also follows. That is, for any $\bar{d}$ with

$$\bar{d} > Y\sqrt{\frac{\bar{\lambda}}{\underline{\lambda}}}, \quad (49)$$

we have $||\hat{e}(t)|| \leq \bar{d}, \forall t \geq t_0 + T(\bar{d}, y)$, with

$$T(\bar{d}, y) = \begin{cases} 0, & y \leq \bar{Y}, \\ \frac{\bar{\lambda} y^2 - \underline{\lambda}\bar{Y}^2}{\lambda \bar{Y}^2 - \frac{1}{4\gamma}}, & otherwise, \end{cases} \quad (50)$$

$$\bar{Y} = \bar{d}\sqrt{\frac{\underline{\lambda}}{\bar{\lambda}}}. \quad (51)$$

The stability of system is guaranteed and tracking error vector $\|\hat{e}\|$ can be made small enough by choosing larger λ and γ.

IV. SIMULATION AND EXPERIMENTAL ANALYSIS

A. PARAMETERS SELECTION AND SIMULATION RESULTS

In the simulation, we choose step signal and sinusoidal signal respectively as the reference signal to verify the three control algorithms: PID control, Model-Based PD (MPD) control without robust component, and the proposed novel robust control (NRC). To distinguish easier in the figures, we call the Model-Based PD control MPD control and the proposed novel robust control algorithm NRC control. The step signal can be described as

$$q^d = \begin{bmatrix} \theta_1^d \\ \theta_2^d \end{bmatrix} = \begin{bmatrix} \frac{\pi}{18} \\ \frac{\pi}{18} \end{bmatrix}, \quad (52)$$

TABLE 1. Parameters of the SCARA robot.

Parameter	Value
$\bar{m}_1(kg)$	0.50
$\bar{m}_2(kg)$	0.50
$m_3(kg)$	2.50
$\bar{m}_4(kg)$	3.00
$I_1(kg \cdot m^2)$	0.32
$I_2(kg \cdot m^2)$	0.06
$c_1(m)$	0.132
$c_2(m)$	0.22
$l_1(m)$	0.351
$l_2(m)$	0.337
$l_3(m)$	0.142

and the sinusoidal signal can be described as

$$q^d = \begin{bmatrix} \theta_1^d \\ \theta_2^d \end{bmatrix} = \begin{bmatrix} \frac{\pi}{6} sint \\ \frac{\pi}{6} sint \end{bmatrix}. \tag{53}$$

The inherent system parameters of the SCARA robot, as the simulation parameters, which are exported from the software CAD and shown in Table 1. Furthermore, the friction force F of (16) is

$$F_i(\dot{q}_i(t)) = [f_{ci} + (f_{si} - f_{ci})e^{-(\dot{\theta}_i/\omega_s)^2}]sgn(\dot{\theta}_i) + f_{vi}\dot{\theta}_i - f_{gi}, \quad i = 1, 2, \tag{54}$$

$$\begin{cases} f_{gi} = s_i e^{-(\dot{\theta}_i/v_i)^2} \\ s_i = sgn(\dfrac{\dot{\theta}_i}{a_i}) f_{si} + f_{ci} l \\ v_i = a_i \omega_s [d \cdot sgn(a) + c \cdot sgn(\dot{\theta}_i)], \quad i = 1, 2 \end{cases} \tag{55}$$

with $f_{si} = [0.4,0.6]^T$, $f_{ci} = [0.32,0.44]^T$, $f_{vi} = [0.04,0.03]^T$, and $\omega_s = 0.04$, $d = 1.16$, $c = 2.08$, $l = 0.18$.

Testing the three control algorithms repeatedly, we select one of the results with a good performance from each algorithm for comparison. The optimal PID parameter are as follows, $P = [120, 95]^T$, $I = [0.1, 0.1]^T$, $D = [20, 22]^T$, whereas the MPD control and the NRC control are finally determined $S = diag[1; 1]$, $P = diag[260; 195]$ and $D = diag[37; 25]$. We choose $\rho = 2$, $\gamma = 1.55$, $\epsilon = 1.5$ as robust term parameters. The uncertainties are assumed as

$$m_1 = \bar{m}_1 + \Delta m_1, \tag{56}$$
$$m_2 = \bar{m}_2 + \Delta m_2, \tag{57}$$
$$m_4 = \bar{m}_4 + \Delta m_4, \tag{58}$$

where

$$\Delta m_1 = \Delta m_2 = 0.05 sint, \tag{59}$$
$$\Delta m_4 = 0.3 sint. \tag{60}$$

The initial time $t_s = 0$ and the initial condition $\hat{e}(0) = [0.1, 0.1, 0, 0]^T$. The simulation results of step response and sinusoid signal tracking are as follows:

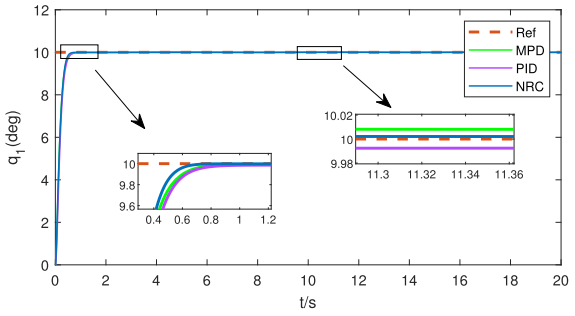

FIGURE 2. Step response curves of joint 1.

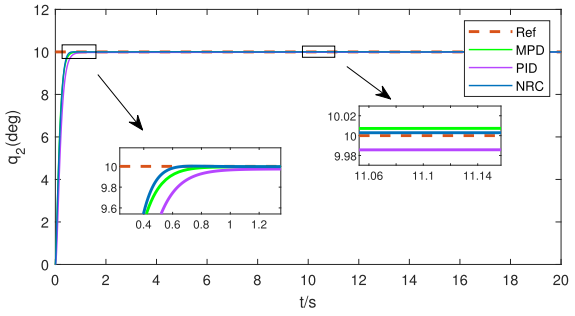

FIGURE 3. Step response curves of joint 2.

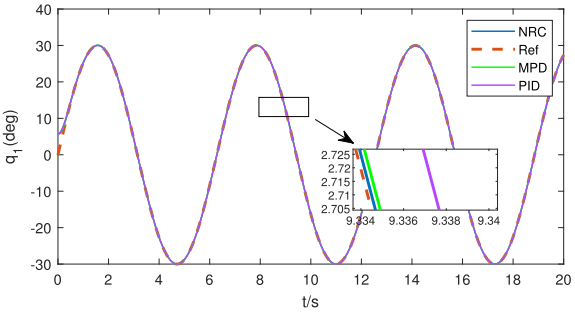

FIGURE 4. The position tracking curves of joint 1.

1) STEP RESPONSE

The results of two joints tracking the reference step signals 10° with three control algorithms are shown in Fig.2 and Fig.3. The step response time with NRC is shorter and the steady-state tracking error is smaller than the others of both joints. Specifically, the response time of the NRC is close to 0.6s, whereas the others are more than 0.8s. The steady-state error with the NRC is −0.002 to 0.004 °, whereas the MPD's is −0.008 ° to 0.009 ° and the PID's is −0.01 ° to 0.02 °.

2) SINUSOID SIGNAL TRACKING

Fig.4-Fig.9 show the sinusoid signal tracking result comparison among three algorithms. From Fig.4 and Fig.5, it can be found that although almost all controllers can quickly track the reference signal at the initial time, the steady-state error with the NRC algorithm is smaller than the others.

B. EXPERIMENTAL PLATFORM AND EXPERIMENTAL RESULTS

Just simulation may not fully indicate the superiority of the proposed control algorithm. In order to ulteriorly verify

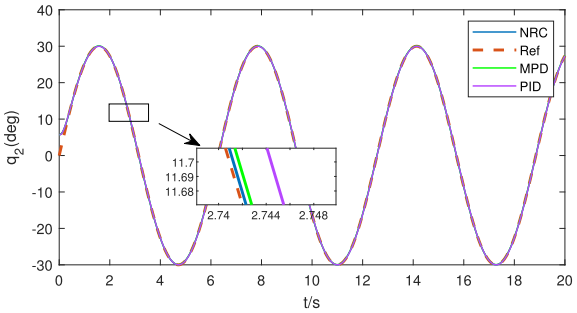

FIGURE 5. The position tracking curves of joint 2.

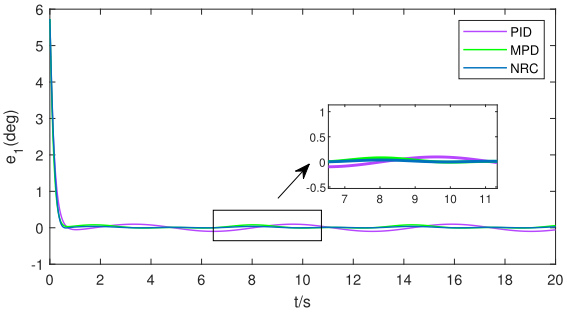

FIGURE 6. The error curves of joint 1.

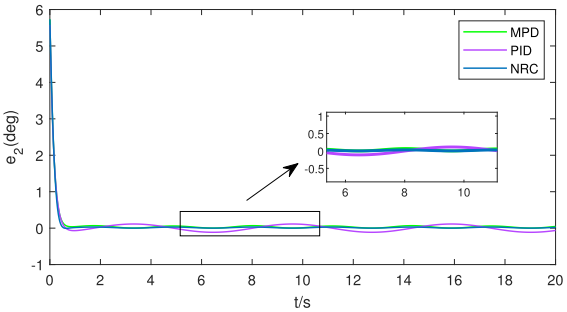

FIGURE 7. The error curves of joint 2.

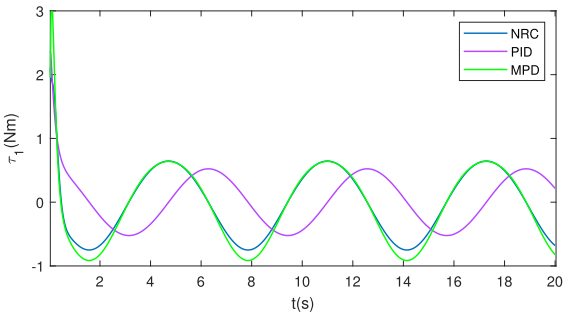

FIGURE 8. The control of joint 1.

that our proposed algorithm is effective, we complete the corresponding dynamics experiments on the SCARA robot platform. Fig.10 shows the experimental equipment, which consists of the SCARA robot, cSPACE control system, computer and cSPACE upper-computer software, motor driver, and so on. The cSPACE control platform is a kind of rapid control prototype system, which adopts the method of real-time simulation and control the hardware in loop to design. It uses the C2000 Support Package

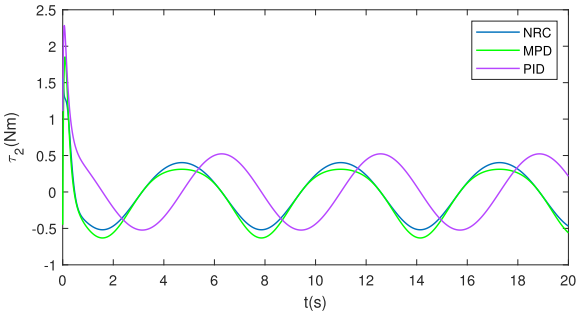

FIGURE 9. The control of joint 2.

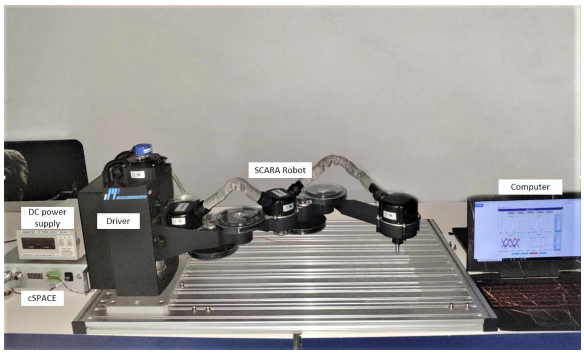

FIGURE 10. Experimental platform of SCARA robot.

provided by the TI company to directly generate the code on MATLAB/Simulink, from which we can realize the combination of computer simulation and real-time control.

The experimental process can be summarized as the following three steps:

Step1: The absolute value encoder collects the motor position signal and feeds it back to the driver.

Step2: The digital signal processor (DSP TMS320F28335) in the cSPACE receives the drive signal and computes it in combination with the control algorithm.

Step3: The calculated control signal is output through CAN communication and then amplified to drive the motor, to realize the motion control of the robot.

1) TRANSIENT PERFORMANCE

Consistent with the simulation, both joints are required to refer to the step signals of 10°. The step response curves of the system with three algorithms are shown in Fig.11 and Fig.12. It can be found that the step response time of NRC is not significantly different from the other two algorithms, since the proposed algorithm is mainly concerned with the steady-state performance of the uncertain system. Specifically, we can get the steady-state errors of the NRC algorithm $e_1 = -0.005°$ to 0, $e_2 = 0$ to 0.003°, whereas the MBD control $e_1 = -0.02°$ to 0, $e_2 = -0.01°$ to 0 and the PID control $e_1 = -0.06°$ to 0, $e_2 = -0.018°$ to 0.

2) STEADY-STATE PERFORMANCE

Fig.13 to Fig.18 show the experimental comparison results of the three different algorithms with no load. To keep consistent

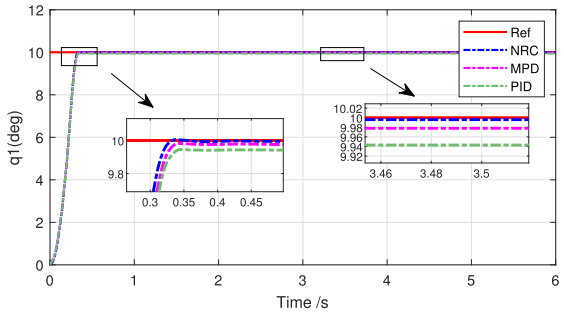

FIGURE 11. Step response curves of joint 1.

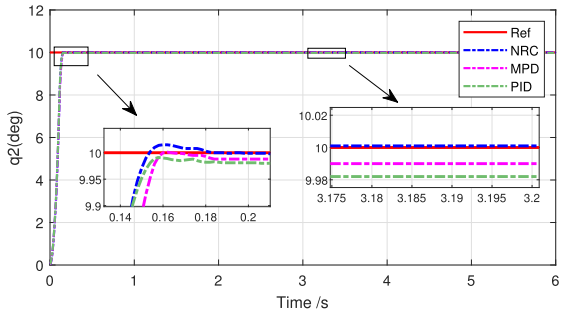

FIGURE 12. Step response curves of joint 2.

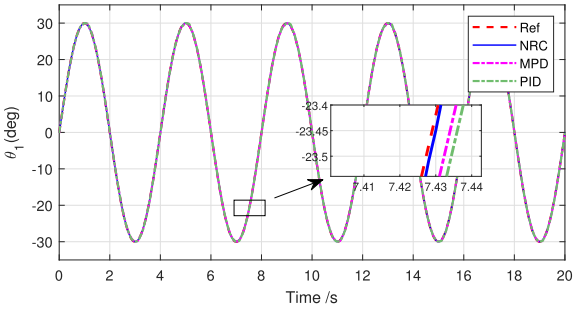

FIGURE 13. The position tracking curves of joint 1.

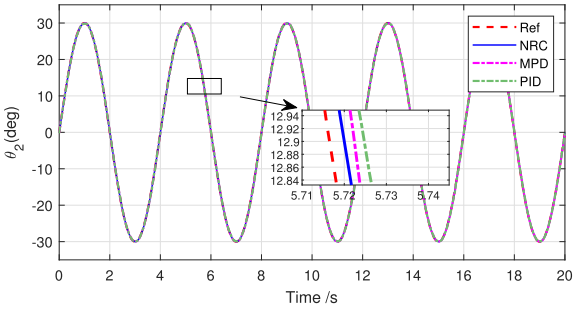

FIGURE 14. The position tracking curves of joint 2.

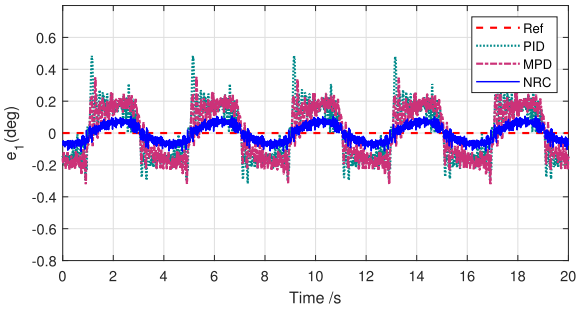

FIGURE 15. The tracking error curves of joint 1.

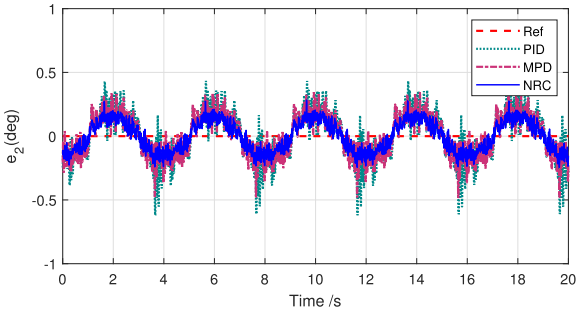

FIGURE 16. The tracking error curves of joint 2.

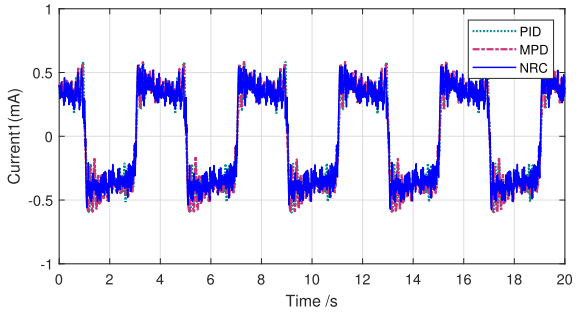

FIGURE 17. The current curves of joint 1.

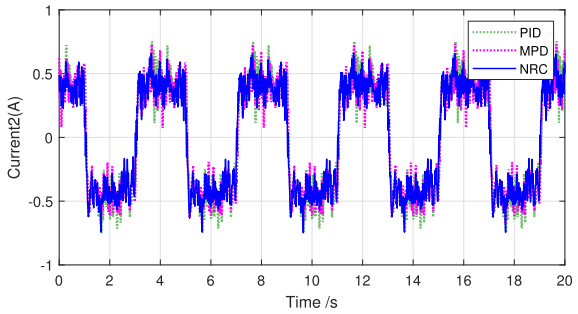

FIGURE 18. The current curves of joint 2.

with the simulation, the amplitude of sinusoidal signals at both joints are 30°. It can be found that the steady-state performance of the NRC algorithm is better than the other two, and one could get more details in the e_1 and e_2 of Fig.15 and Fig.16. The maximum tracking error with the NRC algorithm is minimal.

From Fig.15 and Fig.16, we notice that the maximum of tracking errors always occur when the $\dot{\theta}$ is around zero with all controllers. The reasons may be the gear backlash and Coulomb friction. Fig.19 and Fig.20 show the comparison of tracking error curves with the NRC algorithm which adds a modified Stribeck friction model with Gaussian compensation term, Coulomb-Viscous friction, and no friction respectively. The error curve with Gaussian compensation is smoother and the maximum tracking error is lower than the other two, which reveals the friction model (17) we select in the research has a certain effect on restraining the reversal chattering.

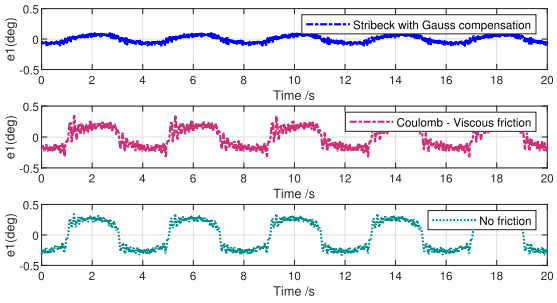

FIGURE 19. The comparison curves of tracking error with different friction models (joint 1).

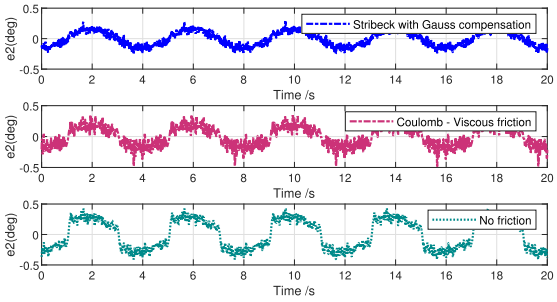

FIGURE 20. The comparison curves of tracking error with different friction models (joint 2).

TABLE 2. Comparisons of steady-state performance without payload.

	Performance	PID	MPD	NRC	Improvement
joint1	RMSE(deg)	0.1721	0.1623	0.1081	37.2%/33.4%
	MAXE(deg)	0.4870	0.3520	0.1850	62.1%/47.4%
joint2	RMSE(deg)	0.1496	0.1344	0.1041	30.4%/22.5%
	MAXE(deg)	0.5875	0.4840	0.2730	53.5%/43.6%

TABLE 3. Comparisons of steady-state performance with different friction models.

	Performance	Without friction	Coulomb-Viscous	Modified Stribeck	Improvement
joint1	RMSE(deg)	0.2331	0.1723	0.1081	53.6%/37.3%
	MAXE(deg)	0.3518	0.3480	0.1850	47.3%/46.8%
joint2	RMSE(deg)	0.2401	0.1596	0.1041	56.6%/34.8%
	MAXE(deg)	0.4840	0.4250	0.2730	43.6%/35.8%

To quantify the steady-state performance of the three algorithms, Table 2 shows the maximum displacement error (MAXE) and the root mean square of displacement error (RMSE) of the three algorithms, which are defined as:

$$MAXE = \max(|e_i|), \tag{61}$$

$$RMSE = \sqrt{\frac{1}{n}\sum_{i=1}^{n} e_i^2}, \tag{62}$$

where e_i denotes the i-th sampled tracking error and n is the number of samples. The improvement refers to the performance improvement of NRC relative to PID and MPD, respectively. Table 2 clearly shows the performance of the three algorithms. The NRC algorithm possesses a smaller RMSE and MAXE than the others. Table 3 shows the performance comparison of RMSE and MAXE.

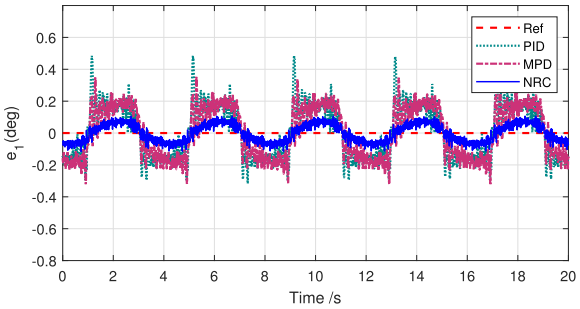

FIGURE 21. The tracking error curves of joint 1 with 0kg payload.

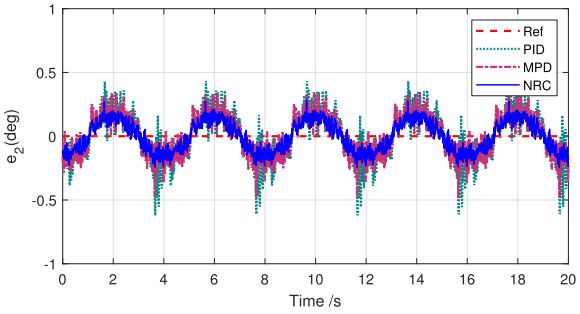

FIGURE 22. The tracking error curves of joint 2 with 0kg payload.

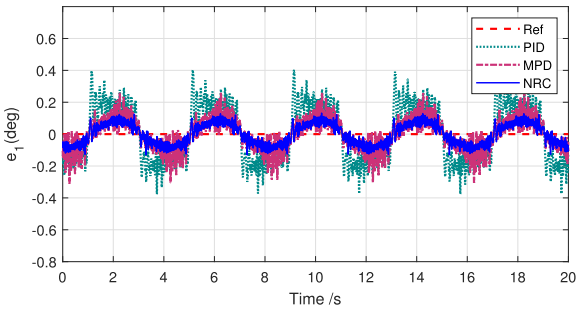

FIGURE 23. The tracking error curves of joint 1 with 0.5kg payload.

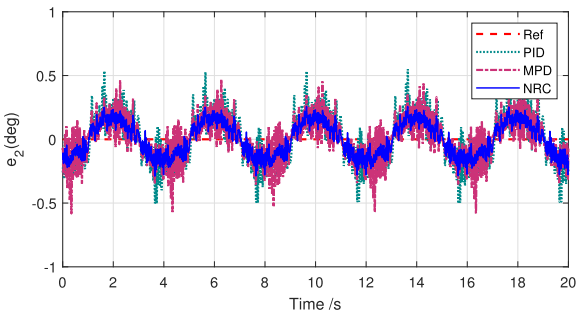

FIGURE 24. The tracking error curves of joint 2 with 0.5kg payload.

The improvement refers to the performance improvement of the modified Stribeck friction model relative to the Coulomb-Viscous friction model and without friction model, respectively. The results also prove the effectiveness of the modified Stribeck friction model.

3) ROBUSTNESS OF LOAD CHANGE

Load variation is one of the main uncertainties of the SCARA robot. The performance of each control algorithm varies

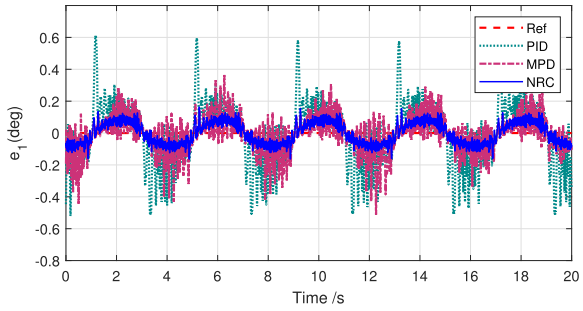

FIGURE 25. The tracking error curves of joint 1 with 1kg payload.

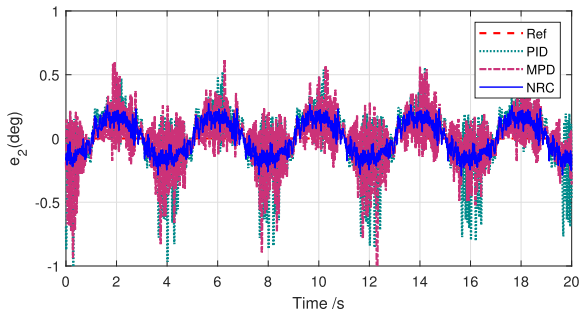

FIGURE 26. The tracking error curves of joint 2 with 1kg payload.

TABLE 4. Comparisons of steady-state performance of the joint 1 with different payload.

Payload	Performance	PID	MPD	NRC	Improvement
0kg	RMSE(deg)	0.1721	0.1623	0.1081	37.2%/33.4%
	MAXE(deg)	0.4870	0.3520	0.1850	62.1%/47.4%
0.5kg	RMSE(deg)	0.1808	0.0997	0.0654	63.8%/34.4%
	MAXE(deg)	0.4020	0.3100	0.1320	67.2%/57.4%
1kg	RMSE(deg)	0.1970	0.1190	0.0683	65.3%/42.6%
	MAXE(deg)	0.6150	0.5120	0.1640	73.3%/68.0%

TABLE 5. Comparisons of steady-state performance of the joint 2 with different payload.

Payload	Performance	PID	MPD	NRC	Improvement
0kg	RMSE(deg)	0.1496	0.1344	0.1041	30.4%/22.5%
	MAXE(deg)	0.5875	0.4840	0.2730	53.5%/43.6%
0.5kg	RMSE(deg)	0.1875	0.1635	0.1284	31.5%/21.5%
	MAXE(deg)	0.6011	0.5830	0.2890	51.9%/50.4%
1kg	RMSE(deg)	0.2405	0.2106	0.1326	44.9%/37.1%
	MAXE(deg)	1.0100	1.2700	0.2940	70.9%/76.9%

with different payloads. Thus, we conduct three comparative experiments with 0kg, 0.5kg, and 1kg payload. Fig.21 to Fig.26 show the comparison results of the three control algorithms. The tracking error under the NRC algorithm just increases a little, whereas the increase of payload has a great impact on the other two algorithms, especially joint 2.

Table 4 and Table 5 show the RMSE and MAXE of the three algorithms with different payloads. The improvement refers to the performance improvement of NRC relative to PID and MPD, respectively. The NRC algorithm, compared with the other two, possesses smaller RMSE and MAXE in each case. Moreover, as the load increases, the performance of the NRC algorithm has improved even more, which means that the NRC algorithm shows better robustness when external disturbances increase.

V. CONCLUSION

We propose a novel practical robust control scheme for the SCARA robot and verify the effectiveness through experiments in this paper. The algorithm is composed of a PD feedback term based on the model and a robust term. The formation of the robust part comprises the upper bound of the uncertainty. To restrain the reversal chattering, we apply the modified Stribeck friction model with Gaussian compensation term as the friction description. The algorithm is demonstrated the guaranteed system performance with the Lyapunov minimax method. Simulation and experimental results prove that the proposed algorithm has a good steady-state performance. Moreover, rapid controller prototyping cSPACE, as the experimental platform, can eliminate the tedious programming work and provide a great convenience for the experiments. The experiments mainly compare the trajectory tracking capabilities of the robot under three algorithms. The results indicate that the proposed algorithm has better robustness, which provides accurate trajectory tracking under the influence of uncertainties. The algorithm could solve the control design problem of similar time-varying nonlinear systems, especially appropriate for engineering applications. We will further consider the effect of electromagnetic interference on the SCARA robot system in future work.

REFERENCES

[1] W.-B. Li, G.-Z. Cao, X.-Q. Guo, and S.-D. Huang, "Development of a 4-DOF SCARA robot with 3R1P for pick-and-place tasks," in *Proc. 6th Int. Conf. Power Electron. Syst. Appl. (PESA)*, Dec. 2015, pp. 1–5.
[2] C. Zhang and Z. Zhang, "Modelling and simulation of SCARA robot using MATLAB/Sim mechanics," in *Proc. IEEE 3rd Adv. Inf. Manage., Commun., Electron. Autom. Control Conf. (IMCEC)*, Oct. 2019, pp. 516–519.
[3] V. M. Hernández-Guzmán and J. Orrante-Sakanassi, "Global PID control of robot manipulators equipped with PMSMs," *Asian J. Control*, vol. 20, no. 1, pp. 236–249, Jan. 2018.
[4] P. J. Gaidhane, M. J. Nigam, A. Kumar, and P. M. Pradhan, "Design of interval type-2 fuzzy precompensated pid controller applied to two-DOF robotic manipulator with variable payload," *ISA Trans.*, vol. 89, pp. 169–185, Dec. 2019.
[5] Y. He, X. Mai, C. Cui, J. Gao, Z. Yang, K. Zhang, X. Chen, Y. Chen, and H. Tang, "Dynamic modeling, simulation, and experimental verification of a wafer handling scara robot with decoupling servo control," *IEEE Access*, vol. 7, pp. 47143–47153, 2019.
[6] X. Yin and L. Pan, "Direct adaptive robust tracking control for 6 DOF industrial robot with enhanced accuracy," *ISA Trans.*, vol. 72, pp. 178–184, Jan. 2018.
[7] Y. Su, C. Zheng, and P. Mercorelli, "Robust approximate fixed-time tracking control for uncertain robot manipulators," *Mech. Syst. Signal Process.*, vol. 135, Dec. 2020, Art. no. 106379.
[8] F. A. Bouaziz, Y. Bouteraa, and N. Derbel, "Control energy comparison between 1st and 2nd order sliding mode approach with application to a scara robot," in *Proc. 13th Int. Multi-Conf. Syst., Signals Devices (SSD)*, 2016, pp. 757–761.
[9] A. Nasirian and M. A. Khanesar, "Sliding mode fuzzy rule base bilateral teleoperation control of 2-DOF scara system," in *Proc. Int. Conf. Autom. Control Dyn. Optim. Techn. (ICACDOT)*, 2016, pp. 7–12.
[10] D. C. Gandolfo, F. G. Rossomando, C. M. Soria, and R. O. Carelli, "Adaptive neural compensator for robotic systems control," *IEEE Latin Amer. Trans.*, vol. 17, no. 04, pp. 670–676, Apr. 2019.

[11] E. O . Freire, F. Guido Rossomando, and C. Miguel Soria, "Self-tuning of a neuro-adaptive PID controller for a SCARA robot based on neural network," *IEEE Latin Amer. Trans.*, vol. 16, no. 5, pp. 1364–1374, May 2018.
[12] G. Nazmara, M. M. Fateh, and S. M. Ahmadi, "A robust adaptive impedance control of robots," in *Proc. 6th RSI Int. Conf. Robot. Mechatronics (IcRoM)*, 2018, pp. 40–45.
[13] V. T. Yen, W. Y. Nan, and P. Van Cuong, "Recurrent fuzzy wavelet neural networks based on robust adaptive sliding mode control for industrial robot manipulators," *Neural Comput. Appl.*, vol. 31, no. 11, pp. 6945–6958, 2019.
[14] W. He and Y. Dong, "Adaptive fuzzy neural network control for a constrained robot using impedance learning," *IEEE Trans. Neural Netw. Learn. Syst.*, vol. 29, no. 4, pp. 1174–1186, Apr. 2018.
[15] F. Fei, H. Hongjie, and G. Zhongtong, "Application of genetic algorithm pso in parameter identification of scara robot," in *Proc. Chin. Autom. Congr. (CAC)*, 2017, pp. 923–927.
[16] G. Khodamipour and M. Yaghoobi, "Decentralized adaptive fuzzy controller by adaptive pso approach for industrial robots," in *Proc. Int. Congr. Technol., Commun. Knowl. (ICTCK)*, 2015, pp. 1–8.
[17] X. Wang, S. Chen, T. Chen, and B. Yang, "Study on control design of a two-wheeled self-balancing robot based on adrc," in *Proc. 35th Chin. Control Conf. (CCC)*, 2016, pp. 6227–6232.
[18] K. Shao, J. Zheng, H. Wang, F. Xu, X. Wang, and B. Liang, "Recursive sliding mode control with adaptive disturbance observer for a linear motor positioner," *Mech. Syst. Signal Process.*, vol. 146, Dec. 2020, Art. no. 107014.
[19] X. Guo, Z. Li, and G. Sun, "The robot arm control based on rbf with incremental pid and sliding mode robustness," in *Proc. WRC Symp. Adv. Robot. Autom. (WRC SARA)*, 2019, pp. 97–102.
[20] G. Khodamipour and M. Yaghoobi, "A new approach to optimal anfis controller on manipulator robots," in *Proc. Int. Congr. Technol., Commun. Knowl. (ICTCK)*, 2015, pp. 9–16.
[21] J. Chi, H. Yu, and J. Yu, "Hybrid tracking control of 2-DOF scara robot via port-controlled Hamiltonian and backstepping," *IEEE Access*, vol. 6, pp. 17354–17360, 2018.
[22] K. Shao, J. Zheng, K. Huang, H. Wang, Z. Man, and M. Fu, "Finite-time control of a linear motor positioner using adaptive recursive terminal sliding mode," *IEEE Trans. Ind. Electron.*, vol. 67, no. 8, pp. 6659–6668, Aug. 2020.
[23] L. Chen, H. Wang, Y. Huang, Z. Ping, M. Yu, X. Zheng, M. Ye, and Y. Hu, "Robust hierarchical sliding mode control of a two-wheeled self-balancing vehicle using perturbation estimation," *Mech. Syst. Signal Process.*, vol. 139, May 2020, Art. no. 106584.
[24] J. Choi, J. Baek, W. Lee, Y. S. Lee, and S. Han, "Adaptive model-free control with nonsingular terminal sliding-mode for application to robot manipulators," *IEEE Access*, vol. 8, pp. 169897–169907, 2020.
[25] J.-J. E. Slotine, *Application Nonlinear Control*, vol. 199. Englewood Cliffs, NJ, USA: Prentice-Hall, 1991.
[26] Y.-W. Tang, H.-X. Sun, X. Li, and J.-Z. Song, "Nonlinear friction modeling for modular robot joints," in *Proc. Mech. Mech. Eng.*, Sep. 2016, pp. 908–915.
[27] Y. H. Chen, "On the deterministic performance of uncertain dynamical systems," *Int. J. Control*, vol. 43, no. 5, pp. 1557–1579, May 1986.
[28] M. Corless, "Control of uncertain nonlinear systems," *J. Dyn. Syst. Meas. Control-Trans. ASME*, vol. 115, Jun. 1993.

SHENGCHAO ZHEN (Member, IEEE) received the Ph.D. degree in mechatronic engineering from the School of Mechanical Engineering, Hefei University of Technology, Hefei, China, in 2013.

From 2011 to 2013, he was a Visiting Scholar with the George W. Woodruff School of Mechanical Engineering, Georgia Institute of Technology, Atlanta, GA, USA, founded by China Scholarship Council. He is currently an Associate Professor with the School of Mechanical Engineering, Hefei University of Technology. His research interests include nonlinear system control theory with applications to multi-agent systems, analytic mechanics, dynamics of multi-body systems, optimal control, robust control, adaptive control, fuzzy engineering, and uncertainty management.

ZIYI ZHAO received the B.E. degree in mechanical design and theory from the School of Mechanical Engineering, Hefei University of Technology, Hefei, China, in 2019, where he is currently pursuing the M.E. degree in mechanical engineering.

His research interests include motion control, nonlinear system control theory with applications to manipulator control, robust control, and uncertainty management.

XIAOLI LIU (Student Member, IEEE) received the B.E. and M.E. degrees in mechanical design and theory from the School of Mechanical Engineering, Hefei University of Technology, Hefei, China, in 2012 and 2017, respectively, where she is currently pursuing the Ph.D. degree.

Her research interests include nonlinear system control theory with applications to motor control, analytical mechanics, multi-agent, and robotics.

FENG CHEN received the Ph.D. degree in physics from the University of Science and Technology of China, Hefei, China, in 2014.

He is currently a Lecturer with the School of Advanced Manufacturing Engineering, Hefei University. He is also a Secretary General with the Anhui Provincial Robot and Intelligent Control Committee. His research interests include information control, fuzzy control, and quantum communication transmission.

HAN ZHAO received the Ph.D. degree in mechanics from Aalborg University, Denmark, in 1990.

He is currently a Professor with the School of Mechanical Engineering, Hefei University of Technology. He is also the Chief Scientist of the National Key Research and Development Program of China and a Leading Scientist of Innovative Research Groups of the National Natural Science Foundation of China. His research interests include mechanical transmission, magnetic machine, vehicles, digital design and manufacturing, information systems, dynamics, and control.

YE-HWA CHEN (Member, IEEE) received the B.S. degree in chemical engineering from National Taiwan University, Taipei, Taiwan, and the M.S. and Ph.D. degrees in mechanical engineering from the University of California at Berkeley, Berkeley, CA, USA.

He is currently a Professor with the George W. Woodruff School of Mechanical Engineering, Georgia Institute of Technology, Atlanta, GA, USA. His research interests include fuzzy dynamical systems, fuzzy reasoning, and modeling and control of mechanical systems.